Korean J. Chem. Eng., 36(4), 540-550 (2019)
DOI: 10.1007/s11814-018-0222-6

pISSN: 0256-1115
eISSN: 1975-7220

Degradation and statistical optimization of 3,5,6-trichloro-2-pyridinol by zero valent iron-activated persulfate

Roaa Mogharbel*, Muqiong Liu, Shengli Zou**, and Cherie Yestrebsky*,†**

*Environmental Chemistry Laboratory, University of Central Florida, 4000 Central Florida Blvd., Orlando, FL 32816, United States
**Department of Chemistry, University of Central Florida, 4000 Central Florida Blvd., Orlando, FL 32816, United States
(*Received 13 October 2018 • accepted 27 December 2018*)

Abstract−The compound 3,5,6-trichloro-2-pyridinol (TCPy), a metabolite of the broad-spectrum organophosphorus insecticide chlorpyrifos, is both more persistent and more water soluble than its parent compound. This difference, which allows TCPy to more readily leach into surface water and groundwater, has led to widespread contamination of TCPy in soils and aquatic environments. In this study, the degradation of TCPy by sulfate radicals was evaluated using zero valent iron activated persulfate in aqueous media. Response surface methodology coupled with Box-Behnken design was applied to evaluate the effects of the independent variables (concentration of zero valent iron, concentration of persulfate, and pH) on the mineralization of TCPy by zero valent iron activated persulfate system. The interactions, coefficients, and residuals of these variables were statically evaluated by analysis of variance. Based on the model, the optimum conditions for maximum TCPy mineralization were determined as 10.4 mM of persulfate, 1.2 g/L of zero valent iron and an initial pH of 3.2. The reaction kinetics of the degradation process were examined as functions of persulfate concentration, zero valent iron concentration, and pH. Results show that zero valent iron activated persulfate can effectively remove TCPy in water with a high mineralization rate of up to 81.1%. The degradation pathways of TCPy were proposed based on the products identified by GC-MS. Calculated ΔG values using density functional theory agreed with the proposed experimental pathway.

Keywords: 3,5,6-Trichloro-2-pyridinol, Persulfate, Sulfate Radical, Zero Valent Iron, Box-Behnken Design

INTRODUCTION

Chlorpyrifos (O,O-diethyl-O-3,5,6-trichloro-2-pyridyl phosphorothionate; CP) is a broad-spectrum insecticide which has been used for agriculture worldwide since 1965, though residential use was banned in the United States in the year 2000 [1]. Although CP has played an important role in the protection of food and feed crops, its excessive use and persistence have caused many environmental concerns, including CP contamination of soil and aquatic environments and measurable CP levels on products for human consumption [2]. CP has been released into the environment through agricultural application, improper disposal, and industrial runoff [3]. Once in the environment, the phosphoester bond of CP is hydrolyzed to 3,5,6-trichloro-2-pyridinol (TCPy), which is the primary by product of CP. Also, photodegradation and microbial degradation of CP both demonstrate the formation of TCPy. TCPy is more persistent and more water soluble than its parent compound, according to the United States Environmental Protection Agency (USEPA) [4] which significantly increases its ability to leach into surface water and groundwater, causing widespread contamination in soils and aquatic environments [5,6]. TCPy has been detected in many places where CP was applied. For instance, TCPy has been identified in such diverse sources as spinach, cauliflower, and potato crops, golf course leachate, and human urine. As one would expect, TCPy has been confirmed to be present in wastewater streams from both chlorpyrifos and methyl-chlorpyrifos manufacturing plants [7].

In the past two decades, advanced oxidation processes (AOPs) have been proven to be effective for the degradation of a wide range of persistent organic contaminants [8,9]. In accordance with their varied natures, AOPs oxidize the original contaminants of concern to form various byproducts and eventually to carbon dioxide and water [9].

Persulfate (PS) has been explored as a suitable oxidizing agent for AOPs that can be activated to generate highly reactive sulfate radicals ($SO_4^{\bullet-}$, SR), which bear a strong redox potential ($SO_4^{\bullet-}+e\rightarrow SO_4^{2-}$, E=2.5-3.1 V, depending on pH). Sulfate radicals demonstrate a higher redox potential than both ozone (E=2.08 V) and hypochlorite (E=1.49 V) [10] while also posing less of a hazard to humans and the environment. SR based AOPs (SR-AOPs) have been shown to be effective in mineralizing a variety of organic contaminants in water and wastewater effluents such as herbicides, industrial chemicals, and pharmaceuticals [9,11,12]. Many activation methods have been developed to activate PS, such as heat, UV, basic conditions, and transition metal ions [9].

$$S_2O_8^{2-}+\text{heat/uv}\rightarrow 2SO_4^{\bullet-} \quad (1)$$

$$S_2O_8^{2-}+Me^{n+}\rightarrow SO_4^{2-}+SO_4^{\bullet-}+Me^{(n+1)+1} \quad (2)$$

Iron [as iron (II), Fe^{2+}] is becoming favored over other common transition metals used in persulfate activation because it has low cost

†To whom correspondence should be addressed.
E-mail: cherie.yestrebsky@ucf.edu
Copyright by The Korean Institute of Chemical Engineers.

and low environmental impact [13] (Eq. (3)). However, rapid scavenging of $SO_4^{\bullet-}$ occurs with excessive Fe^{2+}, which in turn reduces the efficiency of Fe^{2+}/PS on contaminant degradation (Eq. (4)) [9]

$$S_2O_8^{2-}+Fe^{2+}\rightarrow SO_4^{2-}+SO_4^{\bullet-}+Fe^{3+} \quad (3)$$

$$Fe^{2+}+SO_4^{\bullet-}\rightarrow Fe^{3+}+SO_4^{2-} \qquad k=4.6\times10^9\ M^{-1}\ S^{-1} \quad (4)$$

Recently, zero valent iron (ZVI) has been developed as an alternative activator of PS to overcome such a disadvantage. ZVI not only acts as a smooth releasing method of Fe^{2+} but is also able to generate sulfate radicals directly (Eqs. (5) and (6)).

$$Fe^0+2H_2O\rightarrow Fe^{2+}+2OH^-+H_2 \quad (5)$$

$$Fe^0+2S_2O_8^{2-}\rightarrow 2SO_4^{2-}+2SO_4^{\bullet-}+Fe^{2+} \quad (6)$$

This study focused on the complete mineralization of TCPy using PS and Fe. While degradation of CP with SR in thermally- and base-activated PS has been reported [14-16], no studies have reported on the complete degradation of TCPy and its byproducts. No other studies have reported on the degradation of TCPy with Fe and PS. Since CP has been a widely used pesticide and its degradation product TCPy persists in soil and water, new methods must be studied and reported in hopes that a financially feasible technique can eventually be developed for field-scale remediation use. Therefore, we evaluated the removal efficiency of TCPy by means of SR based AOPs at the laboratory scale. The primary objective was to investigate ZVI activated persulfate (ZVI/PS) for the oxidation of TCPy in an aqueous system, as quantified by HPLC/MS. This objective included studying the effect of operational parameters such as initial PS concentration, initial ZVI loading, and solution pH on the degradation kinetics of TCPy. The optimization process of TCPy degradation by ZVI/PS involved using the Box-Behnken experimental design (BBD) and response surface modeling (RSM). GC-MS was used to identify the transformation intermediates and products of TCPy, whereby the proposed transformation pathways were compared to theoretical density functional theory (DFT) calculations.

EXPERIMENTAL

1. Chemicals

Neat TCPy, ammonium acetate ($C_2H_7NO_2$, ≥98%), sodium hydrogen carbonate ($NaHCO_3$, 99.5-100.5%), ferrous sulfate ($FeSO_4\cdot 7H_2O$), 1,10-phenanthroline ($C_{12}H_8N_2$, ≥99%), hydroxylamine hydrochloride ($NH_2OH\cdot HCl$, 98.0%), N-tert-Butyldimethylsilyl-N methyltrifluoroacetamide (MTBSTFA (with 1% t-BDMCS)) were purchased from Sigma Aldrich (USA). Sodium persulfate ($Na_2S_2O_8$, ≥98.0%), potassium iodide (KI, ≥99%), HPLC grade solvent; acetonitrile (CH_3CN, >99.9%), formic acid (HCOOH, ≥99.5%), tert-butyl alcohol (TBA) ($C_4H_{10}O$, >99%) and chloroform ($CHCl_3$, 99.8%) were purchased from Fisher Scientific. Iron particles were purchased from Provectus Environmental Products.

2. Experimental Procedure

These experiments were conducted in 20 mL amber glass vials. A predetermined mass of ZVI particles was added to each of the vials, followed by the addition of TCPy stock solution to a final concentration of 10 mg/L (50 μM) and varying concentrations of PS (2.5-25 mM). Then, the vials were placed on a Thermo Scientific MaxO 4000 orbital shaker table operated at 200 rpm at room temperature for an appropriate amount of time. At designated time points, samples were removed from the shaker table and quenched in an ice bath.

To evaluate the effects of the initial concentration of ZVI on TCPy degradation, additional batch experiments were performed with different ZVI concentrations (0.25-2.5 g/L) under the same experimental conditions as described above, but with predetermined concentration of PS.

To study the influence of the initial reaction pH at various pH values (3.0-12.0), the initial pH of the TCPy solution was adjusted by adding small amounts of 0.1 M H_2SO_4 or 0.1 M NaOH to the desired value before starting the experiment. To prevent potential side reactions between $SO_4^{\bullet-}$ and other species, buffers were not employed in the present study. All solutions were prepared daily using deionized water. All experiments were performed in duplicate.

3. Analysis

The TCPy was analyzed on an Agilent 6230 TOF LC-MS with an Agilent Zorbax SB-C18 analytical column and an Agilent 5977 mass spectrometer (GC/MS) with an RTX-5 column (30 m, 0.25 mm i.d., 0.25 μm df). A mixture of Acetonitrile (ACN) and water was used as the mobile phase at ACN : H_2O ratio of 60 : 40% (v : v) and at a flow rate of 1.0 mL/min in LC-MS. To facilitate the release of TCPy and its byproducts and avoid tailing of the chromatographic peaks, a derivative of TCP was prepared following a modified version of the approach by Li et al. [17]. The derivatization procedure at 50 °C was as follows: 150 μM of MTBSTFA was added to 4 ml of the sample. After one hour, samples were extracted by addition of 5 mL chloroform with 10 mins of stirring, then the chloroform layer was analyzed by GC-MS. In GC/MS, an initial oven temperature of 55 °C was used, and then ramped at 5 °C/min up to 170 °C and held for 1 min following by ramping at 5, 10 and 20 °C/min to 130, 160 and 260 °C, respectively. An ultraviolet-visible light (UV-VIS) spectrometer (Agilent 8453 UV Visible Spectrophotometer equipped with deuterium (UV) and tungsten (visible) lamps) was used to determine the concentration of PS and ferrous ions. The concentration of PS anion was determined following the procedure developed by Liang et al. [18]. Ferrous ions were measured with 1,10-phenanthroline at a wavelength of 510 nm for ferroin absorbance [19]. Ion chromatography was used to measure the release of chloride on DionexIonPac AS4A separation column (250 mm×4 mm). A Shimadzu TOC-L Analyzer (Shimadzu Instruments, Kyoto, Japan) was used to determine the concentration of nonpurgeable (total) organic carbon (TOC). Samples were acidified to pH 2-3 with sulfuric acid prior to analysis. Brunauer-Emmett-Teller analysis of surface area and porosity was accomplished using a Micromeritics ASAP 2020 to determine the BET surface area of the ZVI (BET surface area=3.5878 m^2/g).

4. Computational Method

In the DFT study, all geometries were optimized under B3LYP functional using Gaussian 09 molecular orbital calculation software package. The 6-31G++(d,p) basis set and the Polarizable Continuum Model solvent model were applied to obtain satisfying accuracy. Unless specified, the Gibbs free energy is discussed in this research.

5. Experimental Design

To specify the optimum conditions for the system, the design of

the experiment was structured to determine the common relationship between several process variables that influence the system. Response surface methodology, which is an effective and useful statistical method for improving, developing, and optimizing processes, was employed to process the optimization. In the experimental procedure, Box-Behnken design, a widely used form of RSM, was employed [20]. The Design-Expert (10.0.3) statistical software package was used to determine the total number of experimental runs necessary (N). For development of BBD, N is defined as:

$$N=2k(k-1)+C_0 \quad (7)$$

where k is the number of variables and C_0 is the number of central points.

The experimental design consisted of 17 experiments calculated from Eq. (7), which included twelve factorial points with five center points. The independent variables were set at three different levels, low (−1), medium (0) and high (+1). The ranges and coded levels of the TCPy degradation variables studied are given in Table 1. The predicted response (Y) as a function of the main independent variables was expressed by using a second-order polynomial regression model equation:

$$Y=\beta_0+\sum_{i=1}^{k}\beta_i X_i+\sum_{i=1}^{k}\beta_{ii}X_i^2+\sum_{i=1}^{k}\sum_{j=1}^{k}\beta_{ij}X_iX_j+\varepsilon \quad (8)$$

where β_0, β_i, β_{ii}, and β_{ij} are the regression coefficients representing the constant, the linear, the square, and the interactive effect terms, respectively. X_i and X_j are the coded independent variables, while ε is random error.

The parameters that affect the oxidation of TCPy by ZVI/PS, their interactions, coefficients, and residuals were statically evaluated by analysis of variance (ANOVA), which provides an overall summary for the full model.

Table 1. Experimental ranges and levels of the independent test variables

Variables	Unit	Coded variable level		
		−1	0	1
Persulfate (PS)	mM	5	12.5	20
pH	-	3	7.5	12
ZVI	g/L	0.5	1.5	2.5

RESULTS AND DISCUSSION

1. Effects of Parameters on TCPy Removal

1-1. Effect of PS Concentration

The concentration of PS is an essential factor that affects the oxidation of the contaminants in the ZVI/PS system. Increasing PS concentration is associated proportionally with an increase in SR formation, hence improving the oxidation efficiency. The removal of normalized TCPy concentration over time in a ZVI/PS system with various PS concentrations up to 25 mM is presented in Fig. 1(a). For the range of PS doses employed, TCPy removal was significantly faster with higher PS dose up to 15 mM; further increasing the concentration of PS in the solution decreased the overall removal efficiency of TCPy. In the absence of PS, only 5% of TCPy was removed after 40 minutes of reaction. Although a sudden decrease in the concentration of TCPy occurred in all PS containing

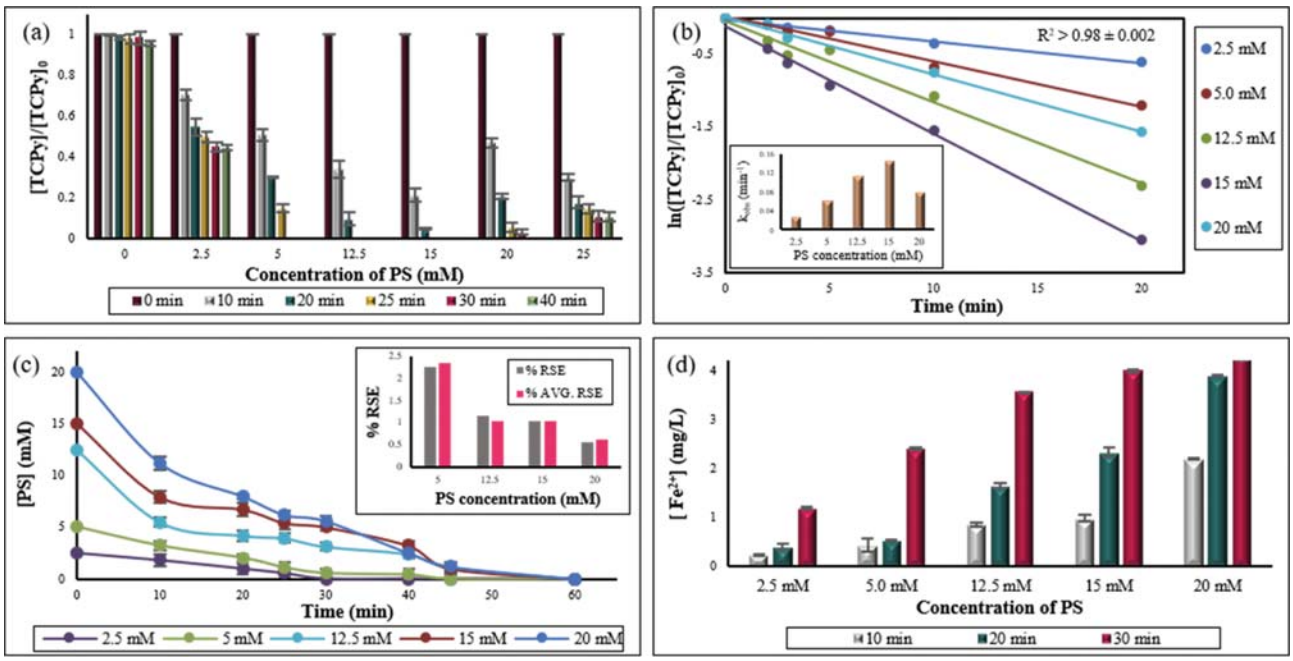

Fig. 1. (a) Effects of PS concentration on TCPy degradation by ZVI activated PS. (b) Pseudo-first-order kinetics of TCPy degradation at different concentrations of PS. Inset: the corresponding rate constants of TCPy removal. (c) PS consumption during the reaction; inset: the reaction stoichiometric efficiencies during the TCPy degradation. (d) The concentration of Fe^{2+} at 10, 20 and 30 min of the reaction. Experimental conditions: $[TCPy]_0$=50 μM; $[PS]_0$=2.5-20 mM; [ZVI]=1.5 g/L; pH=7.5.

systems, complete TCPy removal was not achieved at 2.5 mM PS, and 56% of TCPy remained in the system. As the concentration of PS increased from 5 mM to 15 mM, the reaction time for TCPy removal was reduced and TCPy was successfully oxidized in 30 mins and 25 mins, respectively. High PS dosage enhances TCPy degradation due to the higher number of radicals produced (Eq. (6)). However, when the concentration of PS further increased to 20 mM, the reaction time increased and TCPy was removed after 40 mins of the reaction. Further increasing of the PS concentration to 25 mM lowered the degradation efficiency of TCPy and almost 20% of TCPy remained in the system. This trend can be attributed to the greater production of SR by excess PS, which results in radical-radical reactions (Eq. (9)). Moreover, both Fe(II) and PS may scavenge SR, as demonstrated in Eq. (4) and (10) [11,22]. Given that the rate constant for SR quenching by Fe(II) is a full order of magnitude larger than quenching itself (Eq. (9)), iron is likely more responsible for the reduced activity.

$$SO_4^{\bullet-} + SO_4^{\bullet-} \rightarrow S_2O_8^{2-} \qquad k=4\times10^8\ M^{-1}\ S^{-1} \qquad (9)$$

$$SO_4^{\bullet-} + S_2O_8^{2-} \rightarrow SO_4^{2-} + S_2O_8^{\bullet} \qquad k=6.1\times10^5\ M^{-1}\ S^{-1} \qquad (10)$$

Fig. 1(b) presents the normalized rate constants of TCPy removal at different concentrations of PS. For any specific concentration of PS, TCPy removal exhibited pseudo-first-order kinetics (R^2>0.98± 0.002), which could be described as follows:

$$\ln([TCPy]/[TCPy]_0) = -k_{obs}\cdot t \qquad (11)$$

where k_{obs} (min^{-1}) is the pseudo-first-order rate constant. [TCPy] and $[TCPy]_0$ are the molar concentration of TCPy at times t and 0, respectively. The value of the observed rate constant (k_{obs}) of TCPy removal increased from 2.9×10^{-2} min^{-1} to 1.4×10^{-1} min^{-1} as the concentration of PS increased from 2.5 mM to 15 mM. As PS concentrations increased to 20 mM, the k_{obs} decreased to 7.9×10^{-2} min^{-1} due to the side reaction of SR with higher concentrations of PS as described by Eqs. (9) and (10).

The consumption of PS during the oxidation of TCPy by ZVI/PS for all PS concentrations used is presented in Fig. 1(c). While all PS was consumed ($[PS]_0$=2.5 mM) at 30 min, 66% of PS was consumed with a higher initial concentration of PS ($[PS]_0$=15 mM) in the same time. At initial PS concentration of 12.5 mM and 15 mM, almost 68% and 64% of PS were consumed, respectively, after 25 mins, in which TCPy was completely removed. The PS consumption results demonstrated that the consumption of PS was faster at the beginning of the reaction with higher PS concentration.

The reaction stoichiometric efficiency (RSE), which is the ratio of the molar concentration of oxidized TCPy to the consumed PS, was used in this study to evaluate the utilization efficiency of PS. Actual RSE was calculated for each PS concentration after TCPy was oxidized completely, while RSE average was the mean for each concentration of PS at all sampling times, both are presented in the inset of Fig. 1(c). The results showed that for both actual and average RSE, the highest values were observed for the lowest concentration of PS. For instance, RSE% was increased from 0.571% to 2.25% as the initial PS concentration decreased from 20 mM to 5 mM.

While the concentration of ZVI is the same in all experiments, increasing the PS concentrations contributed to produce more Fe^{2+} in the system (Eq. (6)). Fig. 1(d) shows that the concentration of Fe^{2+} released after ten minutes of reaction increased from 2.4×10^{-1} mg/L at 2.5 mM PS to 2.19 mg/L at 20 mM PS. Similarly, more iron ions were released at higher PS concentrations throughout the course of the experiment. Accordingly, at higher PS concentration, more

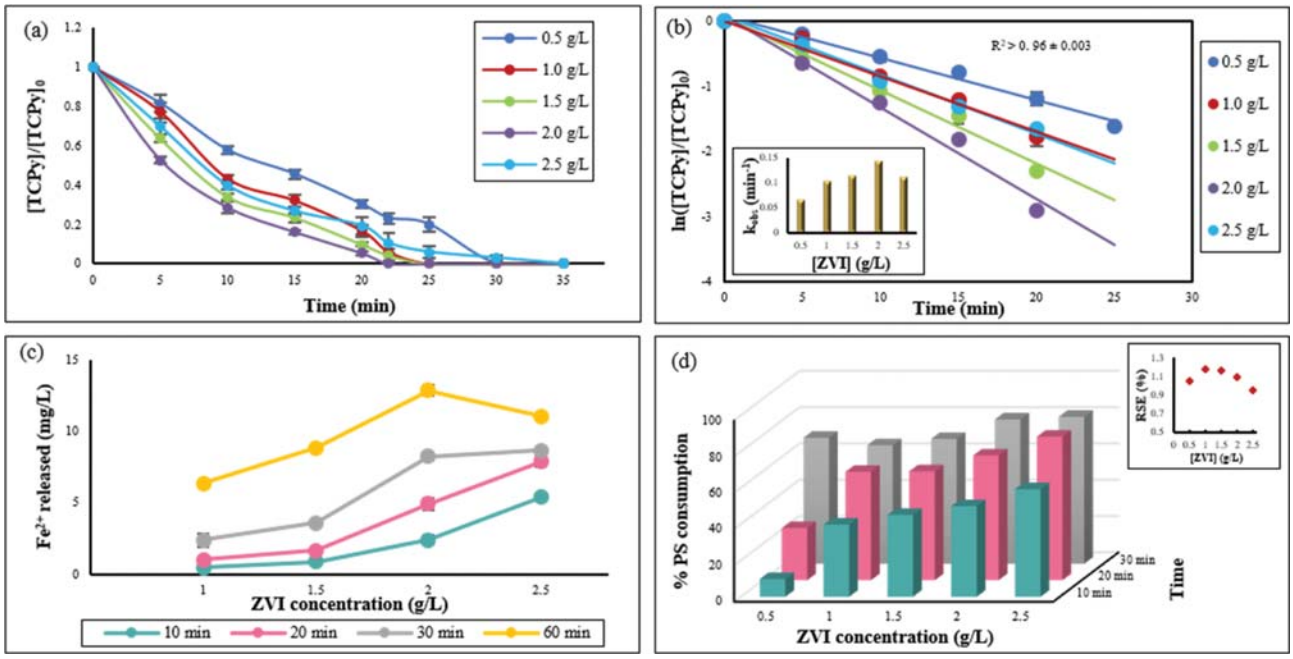

Fig. 2. (a) Effect of ZVI concentration on TCPy degradation by ZVI activated PS. (b) Pseudo-first-order kinetics of TCPy degradation. Inset: plot of k_{obs} vs ZVI concentration. (c) Concentration of Fe^{2+} during the reaction. (d) Consumption of PS at different ZVI concentrations. Inset: RSE% at different ZVI concentrations. Experimental conditions: $[TCPy]_0$=50 μM; $[PS]_0$=12.5 mM; [ZVI]=0.5-2.5 g/L; pH=7.5.

sulfate free radicals would be generated in response to the greater formation of Fe^{2+} activators. This favors the radical reaction with Fe^{2+}, SR, and H_2O (Eqs. (4), (9), and (12), respectively). However, for lower PS concentration, SR generation is less prevalent due to the lower amount of iron ions produced; side reactions are therefore disfavored and the calculated RSE is increased [21,22].

$$SO_4^{\bullet-} + H_2O \rightarrow HSO_4^- + OH^{\bullet} \quad (12)$$

1-2. Effect of ZVI Concentration

ZVI concentration is another essential parameter which influences the degradation efficiency of PS activated by ZVI. Fig. 2(a) shows the role of initial ZVI dosage on the oxidation of TCPy in the ZVI/PS system. It was found that varying the ZVI concentration from 0.5 g/L to 2.5 g/L influenced the TCPy oxidation. As ZVI dosage increased from 0.5 g/L to 2.0 g/L, the removal efficiency of TCPy increased from 77% to 100% after 22 mins of the reaction. The degradation of TCPy is well fitted to a pseudo-first-order kinetics pattern, and the oxidation rate of TCPy was significantly affected by ZVI loading (Fig. 2(b)). The observed first-order rate constants (k_{obs}) went up from 6.4×10^{-2} min^{-1} to 1.4×10^{-1} min^{-1} as the concentration of ZVI increased from 0.5 to 2.0 g/L. However, increasing the ZVI concentration to 2.5 g/L decreased the k_{obs} to 1.1×10^{-1} min^{-1}.

To explore the role of ZVI in ZVI/PS system, the concentration of ferrous ions released during the reaction was investigated. Fig. 2(c) illustrates the released concentration of Fe^{2+} in the ZVI/PS system as a function of reaction time. As the concentration of applied ZVI increased, the concentration of Fe^{2+} in the system increased. For example, at ZVI load (1.0 g/L), a concentration of only 1 mg/L Fe^{2+} was found after 20 mins of the reaction, while 8 mg/L Fe^{2+} was found for the highest ZVI load (2.5 g/L). PS is activated by these Fe^{2+} to generate sulfate radicals that subsequently accelerate the oxidation of TCPy, which can explain the findings in Fig. 2(a). However, increasing the ZVI load causes the release of excessive Fe^{2+} over time, which scavenge the produced sulfate radicals (Eq. (4)), thus reducing the degradation efficiency. The Fe^{2+} release data demonstrates that ZVI plays an integral role in generation of Fe^{2+} in the system. There are many possible routes for the generation of Fe^{2+} in the ZVI/PS system, one being a direct electron transfer from ZVI to persulfate in a Fenton-like reaction incorporating a Haber-Weiss like mechanism [23]. ZVI acts as a reducing agent (E^0=−0.44 V) to provide electrons which reductively decompose persulfate to form sulfate radicals. This direct interaction with persulfate oxidizes iron, resulting in corrosion of ZVI and the release of Fe^{2+} ions (Eq. (6)). Alternatively, Fe^{2+} may be formed as a direct product of corrosion of iron metal under aerobic or anaerobic conditions as described in Eqs. (5) and (13).

$$Fe^0 + H_2O + 0.5\ O_2 \rightarrow Fe^{2+} + 2OH^- \quad (13)$$

The consumption of PS during the reaction at the different applied ZVI dosage is shown in Fig. 2(d). The results indicate that a higher concentration of ZVI consumed more PS. This was likely due to the reaction between PS and Fe^{2+}, which was produced in more quantity with higher ZVI dosage, or the reaction between PS and ZVI itself. The corresponding RSE values are presented in the inset of Fig. 2(d). The RSE was enhanced by increasing the con-

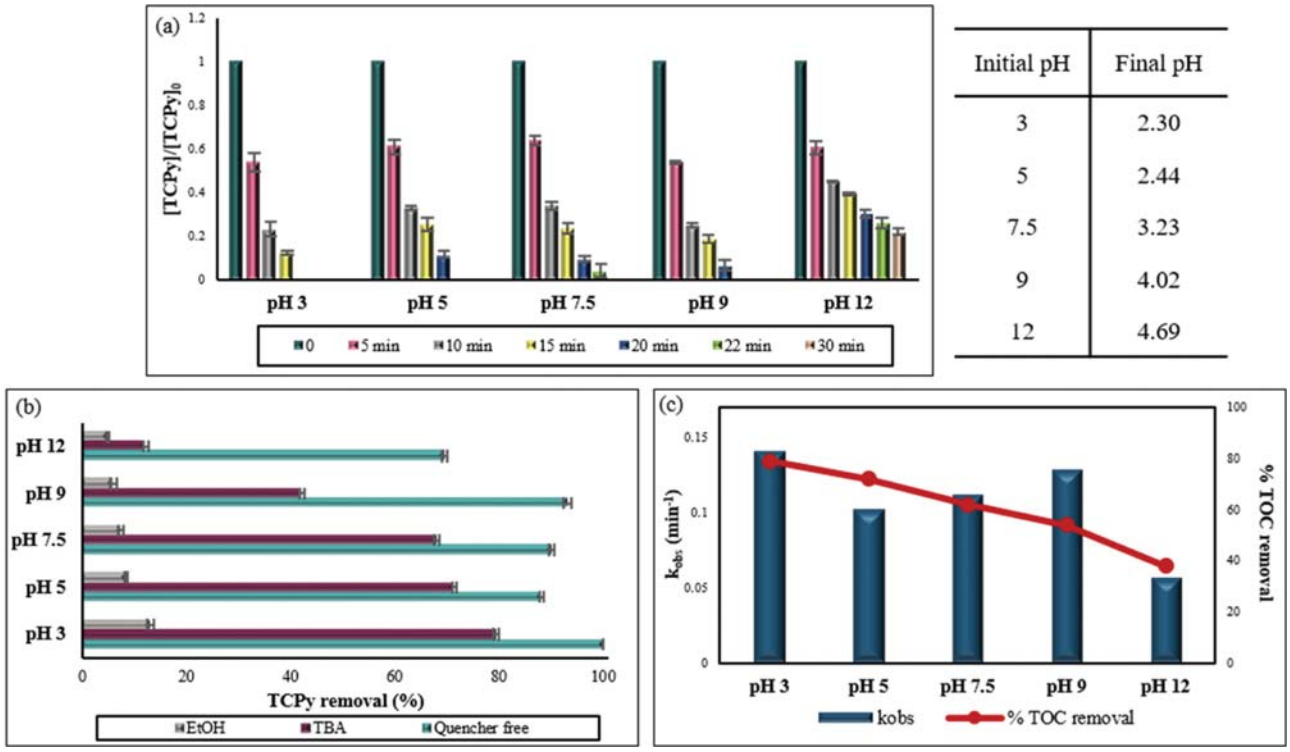

Initial pH	Final pH
3	2.30
5	2.44
7.5	3.23
9	4.02
12	4.69

Fig. 3. (a) Oxidation of TCPy by ZVI/PS at different pH. (b) TCPy degradation in the absence and in the presence of radical scavengers at different pH in ZVI/PS system. (c) Plot of k_{obs} vs pH and %TOC removal after 2 hours of the reaction at different pH. Experimental conditions: $[TCPy]_0$=50 μM; $[PS]_0$=12.5 mM; [ZVI]=1.5 g/L; pH=3-12.

centration of ZVI from 0.5 g/L to 1.0 and 1.5 g/L. However, further increasing ZVI decreased the RSE% which was likely due to the scavenging of SRs by Fe^{2+} (Eq. (4)).

1-3. Effect of pH

Solution pH is an important environmental parameter that may significantly affect the pollutant's degradation as well as the formation of radicals [24]. In the ZVI/PS system, as the solution pH changes the dominant oxidizing species changes. The reaction of sulfate radicals with water at all pH values results in the formation of hydroxyl radicals (HR) (Eq. (14)). Under acidic conditions, sulfate radicals are the primary reactive species; however, all sulfate radicals are converted into hydroxyl radicals in basic conditions (Eq. (15)) [24].

$$SO_4^{\bullet-} + H_2O \rightarrow SO_4^{2-} + OH^{\bullet} + H^+ \quad (14)$$

$$SO_4^{\bullet-} + OH^- \rightarrow SO_4^{2-} + OH^{\bullet} \quad (15)$$

This radical conversion is mainly controlled by Eq. (15) since the rate constant for the reaction in Eq. (14) ($k\ [H_2O] < 2\times10^{-3}\ s^{-1}$) is low compared to the reaction of SR with other organic contaminants [25].

Fig. 3(a) shows the change in normalized TCPy concentrations over time at various initial solution pH values in the range of 3.0-12.0. The oxidation of TCPy in acidic pH resulted in significantly higher efficiency of removal compared to that of basic pH. Complete TCPy removal was achieved after 20, 22 and 30 minutes reaction at pH 3, 5, and 7.5, respectively. The results indicated that acidic conditions are more favorable for TCPy degradation than neutral condition. This favorability might be ascribed to the formation of more Fe^{2+} in acidic solution because of the iron corrosion (Eq. (16)), which in turn generates more SR and enhances the oxidation efficiency.

$$Fe^0 + 2H^+ \rightarrow Fe^{2+} + H_2 \quad (16)$$

Interestingly, enhancement of TCPy oxidation by the ZVI/PS system was observed after increasing the solution pH to 9.0, and the removal of TCPy was achieved after 22 minutes. However, removal efficiencies of TCPy with ZVI/PS system remained poor at higher pH (pH=12).

As mentioned, the dominant oxidizing species change in response to changing pH. Therefore, radical scavenger tests were used to explore the involvement of SR and HR species in the oxidation of TCPy at different pH. Radical scavengers such as ethanol (EtOH) and tert-butyl alcohol (TBA) are usually used to identify the contribution of SRs and HRs to organic contaminant degradation in the SR- AOPs. EtOH with α-H was reported as an active reactant with both SRs and HRs at rate constant of $((1.6\text{-}7.7)\times10^7\ M^{-1}\ S^{-1}$ and $(1.2\text{-}2.8)\times10^9\ M^{-1}\ S^{-1})$, respectively [25]. In contrast, TBA can mainly scavenge HR at second-order rate constant $((3.8\text{-}7.6)\times10^8\ M^{-1}\ S^{-1})$ approximately 1000-fold higher than that with SR $((4.0\text{-}9.1)\times10^5\ M^{-1}\ S^{-1})$ [25]. Therefore, these two alcohols were used as quenching agent, and the oxidation of TCPy was measured at different pH.

As shown in Fig. 3(b), in the quencher-free system, complete removal of TCPy was achieved at pH 3, while treatment with EtOH resulted in poor degradation efficiency of 13.1%. However, treatment with TBA resulted in higher TCPy removal than treatment with EtOH, indicating that in acidic solution SRs were the predominant species. The same trend was observed at pH 5 and pH 7.5. The removal efficiency of TCPy in the presence of TBA decreased as the solution pH increased to 9, indicating the presence of both SR and HR in the system. However, at pH 12 the inhibition of TCPy degradation levels are close by both TBA and EtOH, indicating a greater generation of HR in the system.

According to the radical scavenger test, SR is the predominant species at pH≤7.5, while HR is the predominant species at pH≥9. These results are in accordance with Liang and Su, who identified the presence of SR and HR by using a chemical probe method on heat activated PS system. Their results indicated that in basic conditions HR is the predominant radical, while at near neutral pH, both SR and HR are present. In acidic conditions with pH less than 7, SR is the predominant radical [25]. Additionally, the pH of each system studied decreased significantly over the course of the reaction, as indicated by the final pH values (taken at 30 minutes) in Fig. 3(a). This is likely due to the production of H^+ and consumption of OH^- described in Eqs. (14) and (15), respectively.

These observations can explain the findings in Fig. 3(a). The highest degradation efficiency occurring in acidic conditions can be attributed to the presence of SR. At pH 9, there is increased HR presence, which has a higher redox potential than SR. The increase of HR along with the presence of SR can explain the enhanced degradation efficiency at pH 9. Furthermore, the reactivity of PS would increase in alkaline conditions, which could account for the enhancement of TCPy removal at higher pH [26]. The poor removal efficiency of TCPy at pH 12 can be attributed to the excessive amount of HR which contributed to the reaction of HR with itself, leading to quick loss of the radicals in the solution (Eq. (17)).

$$OH^{\bullet} + OH^{\bullet} \rightarrow H_2O_2 \quad (17)$$

Although the rate constant for TCPy removal is higher at pH 9 than pH 5 and 7.5, the mineralization efficiency of TCPy after one hour of the reaction is lower at pH 9 (Fig. 3(c)). This is likely due to the formation of an oxide layer on the surface of ZVI, which inhibits the complete mineralization of TCPy.

2. Regression Model Representation

As discussed in section 3.1, the removal efficiency of TCPy in ZVI/PS depends on various parameters. Therefore, RSM with BBD was applied to evaluate the effects of the independent variables ([PS], [ZVI], and pH) and to assess the relationships between them on the mineralization of TCPy by ZVI/PS system. Although complete removal of TCPy by ZVI/PS was achieved after 25 mins of reaction, only partial mineralization of TCPy (4.0-32.1%) occurred, depending on process parameters. Thus, mineralization after two hours treatment (up to 81% mineralization) was chosen as an appropriate measure for assessing the combined effect of the selected parameters by RSM.

The experimental design matrix using three factors as independent variables and the response (TCPy mineralization) based on experimental runs proposed by BBD are summarized in Table 2. Design-Expert software indicated that the quadratic model is the most applicable for the degradation of TCPy by ZVI/PS due to its higher R^2 value as well as lower standard deviate on relative to other

Table 2. The BBD design matrix and experimental results for TCPy mineralization by ZVI/PS

Run	Independent variables (coded)			Mineralization (ΔTOC) (%)	
	PS (mM)	pH	ZVI (g/L)	Experimental	Predicted
1	0	1	−1	20.30	25.30
2	0	0	0	70.20	70.50
3	0	−1	−1	81.10	81.97
4	0	0	0	70.40	70.50
5	1	0	1	39.80	42.56
6	0	0	0	69.8	70.50
7	1	−1	0	70.60	72.84
8	0	0	0	71.40	70.50
9	0	−1	1	80.30	75.30
10	0	0	0	70.70	70.50
11	0	1	1	50.00	49.12
12	1	1	0	20.10	18.21
13	−1	1	0	5.90	3.66
14	1	0	−1	30.30	27.19
15	−1	0	1	4.90	8.01
16	−1	0	−1	9.00	6.24
17	−1	−1	0	30.0	31.89

models. The final predicted model in terms of coded factors can be described by the following Eq.:

$$Y=70.5+13.875\ A-20.7125\ B+4.2875\ C-6.6\ AB+3.4\ AC+7.625\ BC-37.8875\ A^2-0.9625\ B^2-11.6125\ C^2 \quad (18)$$

where Y represents the % mineralization of TCPy at 120 min. A, B, and C are the coded values of the initial concentration of PS, pH, and the initial concentration of ZVI, respectively.

3. Statistical Analysis (ANOVA)

ANOVA was used to assess the significance of the fitting of the second-order quadratic model for TCPy degradation by ZVI/PS as shown in Table 3. The sufficiency of the model was confirmed by a model F-value of 92.49 with (Prob>F) less than 0.0001 as presented in Table 3. The F-value (Fisher value) is based on the number of degrees of freedom (df=n−1) and is used to calculate the P-value (probability). High F-values and low P-values indicate stronger evidence against the null hypothesis, which is to say a greater probability of statistical significance. As shown in the ANOVA table, A, B, C, AB, BC, A^2, and C^2 were determined to be statistically significant model terms. All the studied factors, [PS], pH, and [ZVI], had a significant influence on TCPy degradation by ZVI/PS. Moreover, the interaction between PS or ZVI and pH played an important role in the system for the degradation of TCPy. The coefficient of determination (R^2) in the present study for TCPy mineralization (0.9917) indicates that the fitted polynomial equations have a significant relationship with the model. The values of predicted R^2 and adjusted R^2 (0.8682 and 0.9809, respectively) illustrated a reasonable agreement with less than 0.2 difference, which confirmed the model's good predictability. Moreover, the model is adequate because the signal-to-noise ratio obtained in this study is 26.396, which is significantly greater than the minimum desirable value of 4.

Residual analysis was used to further validate this model. First, a normal probability plot of the residuals was generated, which, according to Teh et al., must approximate a straight line to be valid [27]; this condition is satisfied as shown in Fig. 4(a). Additionally, the residuals are well-distributed around the mean response, indicating satisfactory random distribution. Second, predicted responses were plotted against actual responses to confirm good predictability Fig. 4(b).

4. Response Surface Plotting and Optimization of TCPy Mineralization

The following 3D response surface plots with the corresponding contour plots demonstrate the significant interactions between experimental variables by varying two variables at a fixed value while keeping the other variable at the center level (0) [28]. The 3D plots which were generated by using the developed quadratic model are presented in Fig. 5. These surfaces illustrate that the interactions between ZVI and pH and between pH and PS have stronger influ-

Table 3. ANOVA for response surface quadratic model of TCPy mineralization

Source	Sum of square	df	Mean square	F-value	P-value	
Model	12456.41	9	1384.05	92.49	<0.0001	Significant
A	1540.13	1	1540.13	102.92	<0.0001	
B	3423.06	1	3432.06	229.36	<0.0001	
C	147.06	1	147.06	9.83	0.0165	
AB	174.24	1	174.24	11.64	0.0113	
AC	46.24	1	46.24	3.09	0.1222	
C^2	232.56	1	232.56	15.54	0.0056	
A^2	6044.05	1	6044.05	403.91	<0.0001	
B^2	3.90	1	3.90	0.2607	0.6254	
C^2	567.79	1	567.79	37.94	0.0005	
Residual	104.75	7	14.96			
Lack of fit	103.31	3	34.44	95.66	0.0004	Significant
Pure error	1.44	4	0.3600			
Total	12561.16	16				

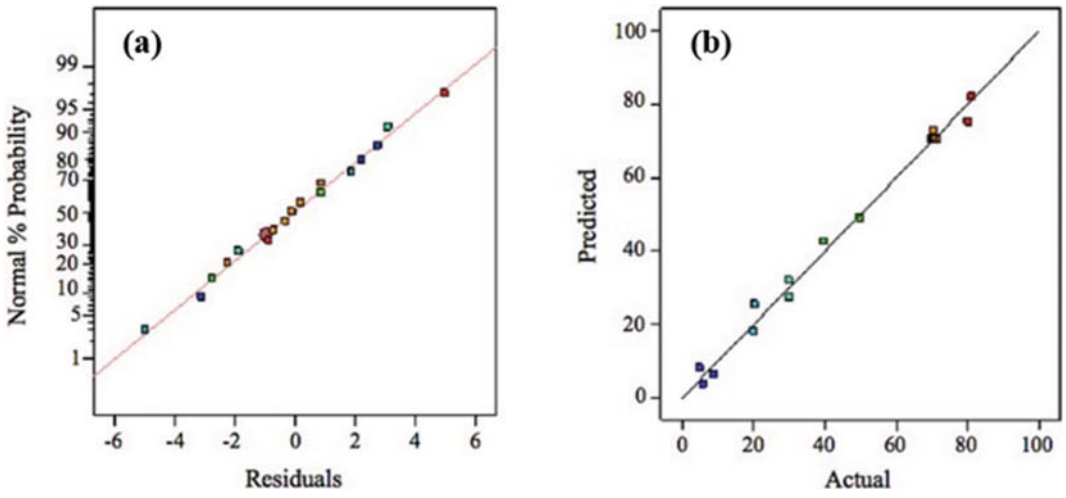

Fig. 4. Residual analysis for TCPy mineralization. (a) Normal plot of residuals (b) predicted response versus actual response.

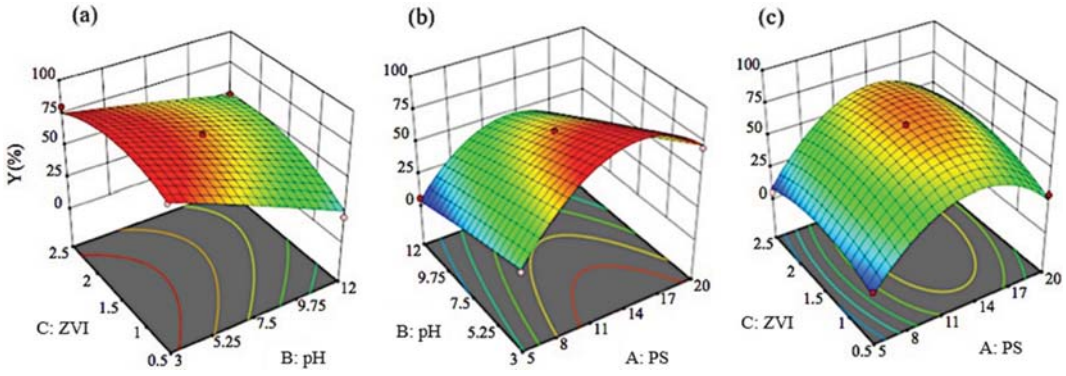

Fig. 5. Response surface graphs of TCPy mineralization by ZVI/PS.

ence on TCPy mineralization than the interaction between ZVI and PS. Additionally, pH has greater influence on TCPy mineralization than ZVI (Fig. 5(a)), and the highest removal efficiency was observed under acidic conditions. The combined influence of pH and the concentrations of PS showed that as PS concentration increased from a low to a moderate value within the experimental range, the mineralization of TCPy increased; however, higher PS concentration decreased the mineralization efficiency (Fig. 5(b)). At low PS concentration, even under acidic conditions, poor mineralization of TCPy was observed indicating that the influence of

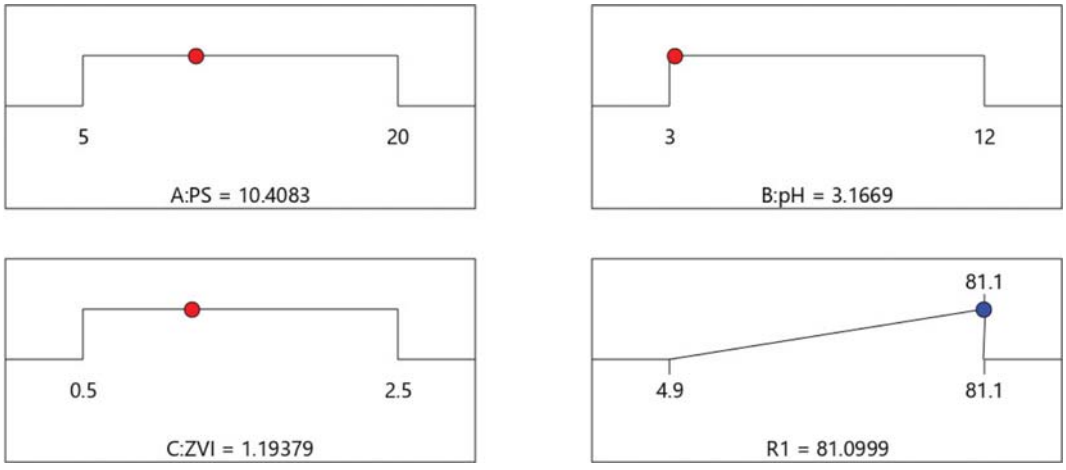

Fig. 6. Desirability ramp for numerical optimization of the TCPy mineralization.

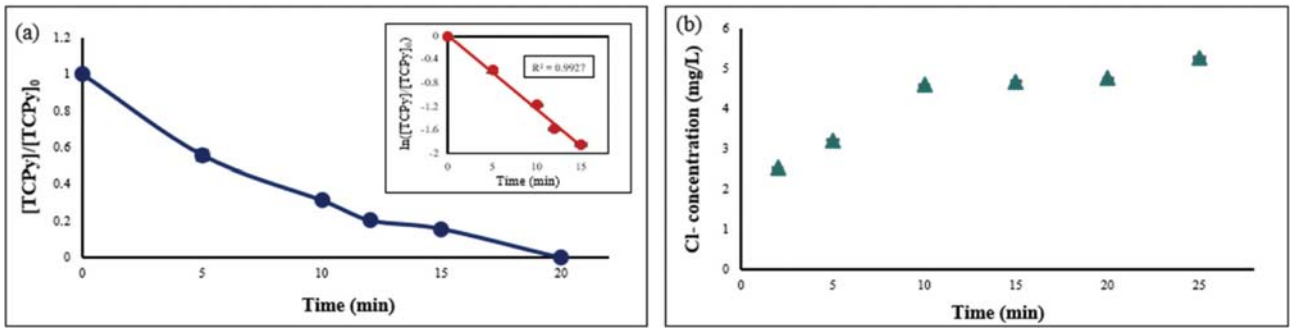

Fig. 7. (a) TCPy oxidation by ZVI/PS at optimal condition. Inset: Pseudo-first-oder kinetics of TCPy degradation. (b) Chloride release during the oxidation of TCPy by ZVI/PS.

PS on TCPy mineralization is greater than that of pH. The combined influence of the concentrations of ZVI and PS showed that the moderated concentration of ZVI and PS within the experimental range contributed to the highest mineralization efficiency of TCPy (Fig. 5(c)). These observations are similar to the finding in the effect of parameters on TCPy removal. Therefore, they can be explained as discussed previously in section 3.1.

Numerical optimization was carried out using Design-Expert software to determine the optimum conditions for the highest mineralization efficiency of TCPy (Fig. 6). All parameters were selected to be within the experimental range, while the response was set to maximum. The optimum conditions that led to maximum TCPy mineralization observed in this study (81.1%) were determined to be 10.4 mM PS concentration, 1.2 g/L initial ZVI concentration, and an initial pH of 3.2 with desirability function value of 1.000. To validate the prediction, an additional experiment was performed in duplicate using the predicted optimal condition. The values of TCPy mineralization obtained in these experiments were 72% and 79.4% with an average of 75.7%. The obtained experimental values and predicted response values were in close agreement, indicating the validity of this prediction.

The degradation of TCPy by ZVI/PS under the optimum conditions suggested by the RSM was studied and the results are presented in Fig. 7. Complete TCPy removal was achieved after 20 mins of reaction, and the TCPy removal exhibited pseudo-first-order kinetics with k_{obs} of 1.254×10^{-1} min^{-1} (Fig. 7(a)). The release of chloride ions during the reaction was measured as presented in Fig. 7(b). The data demonstrated that complete dechlorination of TCPy was achieved since the theoretical release of chloride in 10 mg/L of TCPy after complete dechlorination is 5.36 mg/L.

5. Identification of Degradation Intermediates and Proposed Degradation Pathway

It was reported that the interaction of SR with aromatic compounds results in the formation of carbon-centered radicals by electron transfer from the organic compound to the SR [29]. Therefore, we predict that SR reacts with TCPy via addition to the C_2-C_6 position in an unstable form. Then, the elimination of the sulfate group, which is a good leaving group, results in the formation of a hydroxycyclohexadienyl-like radical, followed by hydroxylation via hydrolysis to form 3,5-dichloro-2,6-dihydroxypyridine, 3,6-dichloro-2,5-dihydroxypyridine or 5,6-dichloro-2,3-dihydroxypyridine as initial transformation products.

Experimentally, 5,6-dichloro-2,3-dihydroxypyridine was identified as one of the major transformation products. This compound was also detected as a byproduct in the photolytic and photocatalytic degradation of TCP in water by Žabar et al. [7]. Feng et al.

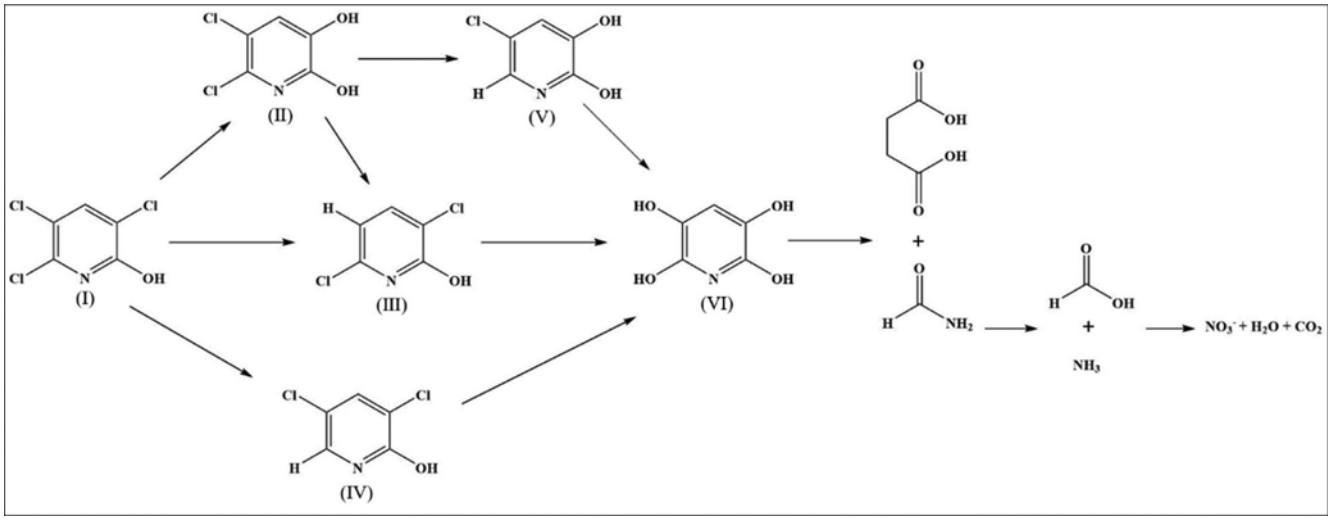

Fig. 8. Degradation pathway for TCPy by ZVI/PS.

also identified 3,5-dichloro-2,6-dihydroxypyridine and 3,6-dichloro-2,5-dihydroxypyridine in addition to 5,6-dichloro-2,3-dihydroxypyridine as byproducts of photolytic degradation of TCPy [30]. However, no experimental evidence for the formation of 3,5-dichloro-2,6-dihydroxypyridine or 3,6-dichloro-2,5-dihydroxypyridine was observed in this study. Since the latter compounds were not observed in this experiment, the formation of the observed 3,5-dichloro-2-hydroxypyridne and 3,6-dichloro-2-hydroxypyridne could be due to the hydrodechlorination of TCPy.

According to the experimentally identified byproducts, a possible degradation pathway of TCPy by ZVI/PS is proposed in Fig. 8. Several possible pathways exist to produce the observed formamide and succinic acid. The reaction of TCPy with water (hydrolysis) results in the formation of 5,6-dichloro-2,3-dihydroxypyridine (II) via nucleophilic substitution on position C_3. The dechlorination of (II) on position C_6 results in the formation of 5-chloro-2,3-dihydroxypyridine (V) followed by dechlorination-hydroxylation processes to form (VI). The hydrodechlorination of (I) results in the formation of (III) and (IV), followed by sequential hydrolysis steps to form (VI). Also, (III) can be formed from hydrodechlorination of II. (VI) in turn is converted to succinic acid and formamide. While the detail of this mechanism is unclear, the formation of succinic acid and formamide suggests a possible retrograde [4+2] cycloaddition (i.e., reverse Diels-Alder) reaction. The formamide decomposes in water to produce formic acid and ammonia, which converts to nitrate [31], while formic acid is further converted to carbon dioxide and water. Although (VI) was not observed in this study, it is predicted to be formed before the ring cleavage.

Gaussian 09 molecular orbital calculation software with B3LYP method was used to calculate the free energies (ΔG) of the reaction to track the oxidation pathways of TCPy by SR before the ring cleavage. The results of calculated ΔG as presented in Table 4 agree with the experimental pathway.

CONCLUSION

ZVI is effective for activating persulfate for degradation of TCPy in water. Increasing the concentration of ZVI and PS increased the rate of TCPy removal; however, higher [PS] or [ZVI] decreased the TCPy oxidation rate. Acidic pH is more favorable toward the TCPy degradation rate than basic pH. For any particular [PS], [ZVI] and pH the removal of TCPy in ZVI/PS exhibited a pseudo-first-order kinetics pattern. Process optimization of the experimental factors ([PS], [ZVI], and pH) was carried out by means of response surface methodology based on Box-Behnken design with TCPy mineralization after two hours chosen as the response. The significance of the fit for the second-order quadratic model for TCPy mineralization was obtained by ANOVA, yielding coefficient of determination (R^2) of 0.9917. The 3D plots show TCPy mineralization was influenced by the combined effect of ZVI and pH as well as between PS and pH. To determine the optimum conditions for the system, desirability function was performed and maximum TCPy mineralization (80.1%) was found at optimum process conditions (10.4 mM PS concentration, 1.2 g/L initial ZVI concentration, and an initial pH of 3.2). These values were further validated by performing duplicate experiments and were found to agree with model predictions. The kinetics of the optimized condition was studied and showed the oxidation of TCPy at this condition is well fitted to a pseudo-first-order model (R=0.99) with removal rate (k_{obs}) of 1.25×10^{-1} min^{-1}. The transformation intermediates and by-products of TCPy oxidation by ZVI/PS were identified by GC-MS, and the proposed transformation pathways (based on experimental analysis) agreed with the theoretical DFT calculations of the free energy values for oxidation reactions of the system.

Table 4. ΔG data of the reaction calculated with Gaussian 09 software with B3LYP method for TCPy and its degradation products

Reactant→Product	ΔG (kcal/mol)
I→II	−16.3
I→III	−28.3
I→IV	−26.3
II→V	−24.9
II→III	−11.9
V→VI	−7.5
III→VI	−20.4
IV→VI	−22.4

REFERENCES

1. A. Grube, D. Donaldson, T. Kiely and L. Wu, US EPA (2011).
2. S. Uniyal and R. K. Sharma, *Biosens. Bioelectron.*, **116**, 37 (2018).
3. S. Khalid, I. Hashmi and S. J. Khan, *J. Environ. Manage.*, **168**, 1 (2016).
4. USEPA (2002). Interim reregistration eligibility decision for chlorpyrifos, Washington D. C. USGPO.
5. S. M. Amer and F. A. Aly, *Mutation Research/Genetic Toxicology*, **279**(3), 165 (1992).
6. J. M. Van Emon, P. Pan and F. van Breukelen, *Chemosphere*, **191**, 537 (2018).
7. R. Žabar, S. Mohamed, A. T. Lebedev, O. V. Polyakova and P. Trebše, *Chemosphere*, **144**, 615 (2016).
8. A. Seidmohammadi, R. Amiri, J. Faradmal, M. Lili and G. Asgari, *Korean J. Chem. Eng.*, **35**(3), 694 (2018).
9. I. A. Ike, K. Linden, J. D. Orbell and M. Duke, *Chem. Eng. J.*, **338**(15), 651 (2018).
10. C. Barrera-Díaz, P. Cañizares, F. J. Fernández, R. Natividad and M. A. Rodrigo, *J. Mex. Che. Soc.*, **58**(3), 256 (2014).
11. X. Wang, J. Min, S. Li, X. Zhu, X. Cao, S. Yuan, X. Zuo and X. Deng, *J. Environ. Chem. Eng.*, **6**(3), 4078 (2018).
12. P. Jeon, S.-M. Park and K. Baek, *Korean J. Chem. Eng.*, **34**(5), 1305 (2017).
13. A. Tsitonaki, B. Petri, M. Crimi, H. Mosbæk, R. L. Siegrist and P. L. Bjerg, *Crit. Rev. Environ. Sci. Technol.*, **40**(1), 55 (2010).
14. L. Zhou, Y. Zhang, R. Ying, G. Wang, T. Long, J. Li and Y. Lin, *Environ. Sci. Pollut. Res. Int.*, **24**(12), 11549 (2017).
15. E. M. Kennedy and J. C. Mackie, *Environ. Sci. Technol.*, **52**(13), 7327 (2018).
16. Z. H. U. Changyin, Z. H. U. Fengxiao, W. A. N. G. Fuwang, G. A. O. Juan, F. A. N. Guangping, Z. H. O. U. Dongmei and F. A. N. G.

Guodong, *Pedosphere*, **27**(3), 465 (2017).
17. R. Li, L. He, T. Zhou, X. Ji, M. Qian, Y. Zhou and Q. Wang, *Anal. Bioanal. Chem.*, **406**(12), 2899 (2014).
18. C. Liang, C. F. Huang, N. Mohanty and R. M. Kurakalva, *Chemosphere*, **73**(9), 1540 (2008).
19. APHA, Standard methods for the examination of water wastewater, 20th Ed., American Public Health Association (1998).
20. S. Das and S. Mishra, *J. Environ. Chem. Eng.*, **5**(1), 588 (2017).
21. X. Wei, N. Gao, C. Li, Y. Deng, S. Zhou and L. Li, *Chem. Eng. J.*, **285**, 660 (2016).
22. A. Ghauch, G. Ayoub and S. Naim, *Chem. Eng. J.*, **228**, 1168 (2013).
23. I. Hussain, Y. Zhang, S. Huang and X. Du, *Chem. Eng. J.*, **203**, 269 (2012).
24. L. W. Matzek and K. E. Carter, *Chemosphere*, **151**, 178 (2016).
25. C. Liang and H.-W. Su, *Ind. Eng. Chem. Res.*, **48**(11), 5558 (2009).
26. Y. Wang, S. Y. Chen, X. Yang, X. F. Huang, Y. H. Yang, E. K. He, S. Wang and R. L. Qiu, *Chem. Eng. J.*, **317**, 613 (2017).
27. C. C. Teh, N. A. Ibrahim and W. M. Z. W. Yunus, *BioResources*, **8**(4), 5244 (2013).
28. H. Kusic, I. Peternel, N. Koprivanac and A. Loncaric Bozic, *J. Environ. Eng.*, **137**(6), 454 (2010).
29. G. P. Anipsitakis, D. D. Dionysiou and M. A. Gonzalez, *Environ. Sci. Technol.*, **40**(3), 1000 (2006).
30. Y. Feng, R. D. Minard and J. M. Bollag, *Environ. Toxicol. Chem.*, **17**(5), 814 (1998).
31. G. K. Low, S. R. McEvoy and R. W. Matthews, *Environ. Sci. Technol.*, **25**(3), 460 (1991).